

MAJOR PAPER

## Preoperative Localization of Parathyroid Adenomas with Diffusion MR Imaging: Readout-segmented versus Single-shot Echo-planar Imaging

Hiroataka Yamamoto<sup>1</sup>, Mami Iima<sup>2,3</sup>, Yo Kishimoto<sup>4\*</sup>, Ayami Ohno Kishimoto<sup>3</sup>,  
Sho Koyasu<sup>2</sup>, Akira Yamamoto<sup>2</sup>, Yoshitaka Kawai<sup>4</sup>, Akira Yoshizawa<sup>4</sup>,  
and Koichi Omori<sup>4</sup>

**Purpose:** To evaluate whether readout-segmented echo-planar imaging (RS-EPI) diffusion-weighted imaging (DWI) can reduce image distortion and improve the lesion identification in parathyroid adenomas (PTAs) compared to single-shot EPI (SS-EPI) DWI, and to determine whether PTAs can be differentiated from other soft tissue structures of the head and neck region by using the apparent diffusion coefficient (ADC) value.

**Methods:** We retrospectively analyzed the preoperative MR images including DWI of 24 patients with surgically confirmed PTA. RS-EPI and SS-EPI DWI were evaluated by two independent readers for the identification of the lesions and distortion. The ADC values of the PTAs were compared with those of thyroid glands and cervical lymph nodes.

**Results:** RS-EPI provided significantly less distortion compared to SS-EPI. RS-EPI tended to have better lesion identification compared with SS-EPI without a statistically significant difference. On SS-EPI, the PTAs had significantly higher ADC values compared with the cervical lymph nodes. On RS-EPI, the PTAs had significantly higher ADC values compared with the thyroid glands and cervical lymph nodes.

**Conclusion:** RS-EPI reduces the DWI distortion in PTAs. The ADC value obtained using RS-EPI enables the differentiation of PTAs from nearby structures, such as thyroid glands and cervical lymph nodes.

**Keywords:** *apparent diffusion coefficient, diffusion-weighted magnetic resonance imaging, parathyroid adenoma, readout-segmented echo-planar imaging*

### Introduction

Primary hyperparathyroidism (PHPT) is a clinical condition characterized by elevated serum parathyroid hormone (PTH),

followed by increased serum calcium (Ca). Patients with PHPT frequently manifest symptoms such as hypercalcemia, anorexia, nausea, and nephrocalcinosis. The treatment for PHPT used to be a total parathyroidectomy, but PHPT is usually caused by a single parathyroid adenoma (PTA),<sup>1,2</sup> and selective parathyroidectomy has been recently preferred for the treatment of single adenomas as a less invasive option.<sup>3,4</sup> For a successful selective parathyroidectomy, accurate imaging techniques are required for the preoperative localization of PTAs. Ultrasonography and technetium 99mTc-sestamibi scintigraphy have often been accepted as the first-line imaging to localize PTAs. When it is difficult to localize the parathyroid lesions only with the first-line imaging, CT and MRI are considered as second-line imaging techniques.<sup>1,5</sup> Recently, the multiphasic CT (4D CT) has made it possible to identify PTAs through their hypervascular perfusion pattern compared with lymph nodes and thyroid gland,<sup>5</sup> however, CT has the disadvantage of ionizing radiation.

MRI has the advantage of the lack of ionizing radiation, and with the introduction of high-field magnetic systems, the

<sup>1</sup>Department of Otolaryngology, Shizuoka City Shizuoka Hospital, Shizuoka, Shizuoka, Japan

<sup>2</sup>Department of Diagnostic Imaging and Nuclear Medicine, Kyoto University Graduate School of Medicine, Kyoto, Kyoto, Japan

<sup>3</sup>Institute for Advancement of Clinical and Translational Science (iACT), Kyoto University Hospital, Kyoto, Kyoto, Japan

<sup>4</sup>Department of Otolaryngology Head and Neck Surgery, Kyoto University Graduate School of Medicine, Kyoto, Kyoto, Japan

\*Corresponding author: Department of Otolaryngology Head and Neck Surgery, Graduate School of Medicine, Kyoto University, 54, Kawahara-cho, Shogoin, Sakyo-ku, Kyoto, Kyoto 606-8507, Japan. Phone: +81-75-751-3346, Fax: +81-75-751-7225, E-mail: y\_kishimoto@ent.kuhp.kyoto-u.ac.jp



This work is licensed under a Creative Commons Attribution-NonCommercial-NoDerivatives International License.

©2022 Japanese Society for Magnetic Resonance in Medicine

Received: November 18, 2021 | Accepted: December 25, 2021

use of MRI for the localization of parathyroid adenomas has been re-assessed as a supplemental imaging modality. The sensitivity of 1.5T MRI for the detection of PTAs was reported to be 43%–71%,<sup>6–8</sup> but since 3T scanners were introduced into clinical practice in the early 2000s, the higher signal-to-noise and contrast-to-noise ratios have improved the sensitivity of MRI to 97.8%.<sup>1</sup> However, some limitations remain because the MR appearance of PTAs overlaps considerably with those of cervical lymph nodes and an ectopic thyroid gland, which leads to difficulties in distinguishing PTAs from other structures in the neck.

The measurement of the apparent diffusion coefficient (ADC) value in diffusion-weighted imaging (DWI) has been reported to be helpful in distinguishing parathyroid tissues from other soft-tissue structures of the head and neck region.<sup>9</sup> Single-shot echo-planar imaging (SS-EPI) has been the most widely used DWI sequence. However, SS-EPI suffers from susceptibility artifacts due to inhomogeneities in the static magnetic field, leading to geometric distortion, signal dropout, and image blurring, which occur especially at higher field strengths,<sup>10</sup> and thus, the detection of PTAs by DWI remains challenging. To overcome this weakness, readout-segmented echo-planar imaging (RS-EPI) was developed; with this imaging modality, there is a substantial reduction in the distortion and blurring caused by T2\* decay during the readout.<sup>11,12</sup> RS-EPI is expected to improve the diagnostic accuracy of detecting PTAs on DWI as it provides less distortion, and its advantages are reported in some organs including the head and neck.<sup>13–15</sup>

However, to our knowledge, there is no literature focusing on the usefulness of 3T RS-EPI for the localization and distinction of PTAs. We conducted the present retrospective study to determine whether 3T RS-EPI can reduce image distortion and improve the lesion identification in PTAs compared to 1.5T SS-EPI, and to determine whether PTAs can be differentiated from other soft-tissue structures of the head and neck region by using the ADC value.

## Materials and Methods

### MRI examination

The MRI examinations in this study were performed with a 1.5T MRI system (Avanto or Trio, Siemens, Erlangen, Germany) or a 3T MRI system (Prisma or Skyra, Siemens). The parameters for the DWI sequences are summarized in Table 1.

### Setting and Participants

A total of 34 patients with PTA who underwent an MRI examination for the preoperative diagnosis of PTA at Kyoto University Hospital (Kyoto, Japan) during the period from January 2012 to March 2020 were examined. We obtained ethical approval for this study from the Institutional Review Board of our hospital (Ref No: R0281). SS-EPI at 1.5T was

**Table 1** Parameters for DWI

	SS-EPI (1.5T)	RS-EPI (3T) <sup>††</sup>
b-value, sec/mm <sup>2</sup>	0, 1000	0, 1000
FOV	180*180	211*220
Matrix	192*192 <sup>†</sup>	142*148
TR	5900	4100
TE	81	54
Slice thickness, mm	4	3
Fat suppression	STIR	SPAIR
Averages	4	1
Acquisition time, min:sec	2	2:15

<sup>†</sup>The matrix for SS-EPI is interpolated. <sup>††</sup>Five readout segments are used. RS-EPI, readout-segmented echoplanar imaging; SS-EPI, single-shot echo-planar imaging.

performed in eight patients during the period January 2012 to November 2017, and RS-EPI at 3.0T was performed in 26 patients during the period July 2014 to March 2020. All patients underwent a parathyroidectomy, and the resected specimens were histologically evaluated. Of the 34 patients, 10 patients were excluded from this study for the following reasons: the lesion was not detectable on MRI (n = 3), DWI data were obtained using a different protocol (n = 5), and the presence of severe motion (n = 2). The remaining 24 patients were enrolled. Their clinical information, including the results of imaging examinations, was retrospectively reviewed.

### Analysis of image quality and distortion

Board-certified radiologists A and B independently evaluated the image quality and the distortion of parathyroid lesions on DWI. They had access to other MR images (T2- or T1-weighted images or STIR images) for a reference. They were informed that the DWIs were acquired for the preoperative evaluation of PTA, and they were unaware of any other radiologic information. Structural identification and geometric distortion were evaluated using a reported five-point scale (Table 2).<sup>13</sup>

### Measurements of ADC values

ADC measurements of the lesions were performed on the ADC map that contained the largest lesion cross-section, using circular ROIs with a mean area of 10 mm<sup>2</sup>. Each ROI was carefully drawn within the solid part of the lesion to exclude artifacts and areas of cyst and/or necrosis. The ADC values of each patient's cervical lymph nodes and thyroid glands were also measured.

### The DWI statistical analysis

The inter-observer variability between the two radiologists was evaluated using inter-rater agreement (Kappa coefficient). As described,<sup>16</sup> the results were interpreted as follows:

**Table 2** Scales for structure identification and geometric distortion on DWI (modified from ref. 13)

Scales for structural identification
4 Excellent: Perfectly demarcated contour and very good contrast with surrounding structure
3 Good: Almost good contour, but partially (< 50%) mixed with the background
2 Fair: Organ/node can be discriminated from surrounding structures, while more than half of the contour is mixed with the background
1 Faint: Structures of organ/nodes are ill-defined, but can be identified by faint contrast with surrounding structures
0 Unidentifiable: Cannot identify any structures
Scales for geometric distortion
4 High geometric accuracy and almost no distortion
3 Faint distortion: Organ/node slightly tilts, but its convexity is almost the same as that of T2-weighted turbo spin-echo sequence (TSE) image
2 Moderate distortion: Convexity is less pronounced or lost compared to that of a T2-weighted TSE image
1 Intense distortion: Convexity is opposite compared to that of a T2-weighted TSE image, or severe dislocation exists
0 Impossible to evaluate, or unidentifiable

values  $\leq 0$  indicate no agreement; 0.01–0.20 indicate none to slight agreement, 0.21–0.40 = fair agreement, 0.41–0.60 = moderate, 0.61–0.80 = substantial, and 0.81–1.00 = almost perfect agreement.<sup>17</sup> The ADC values of the parathyroid lesions, thyroid glands, and cervical lymph nodes were analyzed using the Friedman test with Bonferroni correction, and the scores of structure identification and geometric distortion on SS-EPI and RS-EPI were compared using the median test. In both tests,  $P$  values  $< 0.05$  were considered significant. All statistical analyses were performed with EZR (Saitama Medical Center, Jichi Medical University), which is a graphical user interface for R (ver. 2.13.0; The R Foundation for Statistical Computing, Vienna, Austria).<sup>18</sup>

## Results

### *Patients and lesions*

The patient and lesion characteristics are summarized in Table 3. The SS-EPI group was two males and six females (mean age 64 years, range 48–76 years), and the RS-EPI group was six males and ten females (mean age 55.6 years, range 25–80 years). All patients underwent parathyroidectomy, and all lesions were pathologically diagnosed as parathyroid adenomas, and there were no significant differences in patient or lesion characteristics between the two groups.

### *Assessments of structure identification and distortion*

The Kappa values between the two readers revealed substantial-to-perfect agreement (structure identification provided by SS-EPI: 0.73, distortion by SS-EPI: 1, identification by RS-EPI: 0.75, and distortion by RS-EPI: 0.82). The mean scores of structure identification and geometric distortion for SS-EPI and RS-EPI by the two readers are shown in Table 4.

**Table 3** Patient and lesion characteristics

	SS-EPI	RS-EPI	$P$ -value
No. of patients	8	16	
Sex			0.667
Male	2	6	
Female	6	10	
Mean age (range), yrs	64.0 (48–76)	55.6 (25–80)	0.191
Location of lesion			
Right superior	1	4	
Right inferior	2	5	
Left superior	1	0	
Left inferior	4	7	
Size of lesion, mm	19.3 (10–25)	19.0 (8–30)	0.92

Comparisons between the SS-EPI and RS-EPI were performed by Chi-square test for sex, and by median test for age and size of lesion. RS-EPI, readout-segmented echoplanar imaging; SS-EPI, single-shot echo-planar imaging.

The distortion scores for RS-EPI were significantly higher than those for SS-EPI (all  $P$  values were  $< 0.05$ ), indicating lower distortion, and the image quality provided by RS-EPI was better than that obtained with SS-EPI. The results of the median test of the structure identification scores tended to be higher with RS-EPI than SS-EPI; however, the difference did not reach statistical significance.

### *Representative cases*

Representative cases of SS-EPI and RS-EPI are shown in Figs. 1, 2, and 3. A 67-year-old woman was diagnosed as

**Table 4** Evaluation of structural identification and geometric distortion using a five-point scale

	Reader 1			Reader 2		
	SS-EPI	RS-EPI	<i>P</i> -value	SS-EPI	RS-EPI	<i>P</i> value
Identification of structure	1.63 ± 0.92	2.44 ± 1.09	0.085	1.50 ± 0.93	2.38 ± 1.02	0.054
Geometric distortion	1.38 ± 0.92	2.38 ± 0.96	0.023*	1.38 ± 0.92	2.38 ± 0.89	0.017*

Data are mean ± SD. Comparisons between SS-EPI and RS-EPI were performed by median test. \**P* < 0.05.

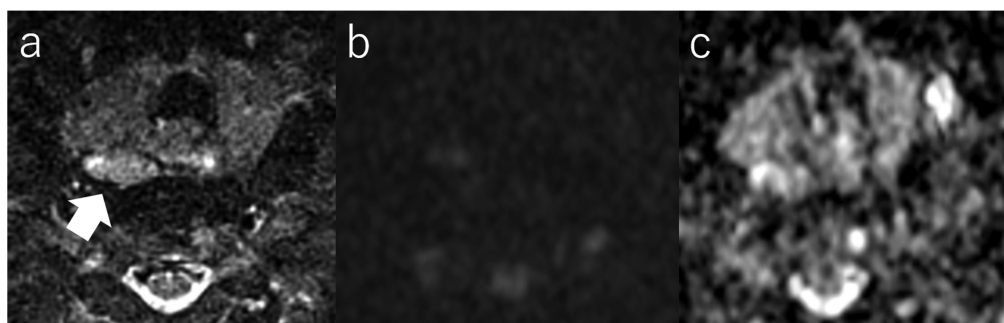


**Fig. 1** Representative SS-EPI images of a 67-year-old woman with primary hyperparathyroidism. **a:** STIR: A high-intensity mass on STIR was detected behind the right lobe of the thyroid gland. **b:** DWI with SS-EPI: A faint high-intensity lesion on DWI was detected in the corresponding location on STIR. The image was scored to be impossible to evaluate by two readers. **c:** ADC map: A high value was detected on the ADC map. The lesion was diagnosed as a PTA of the right superior gland. A 21 × 16 × 17 mm PTA was confirmed at surgery.

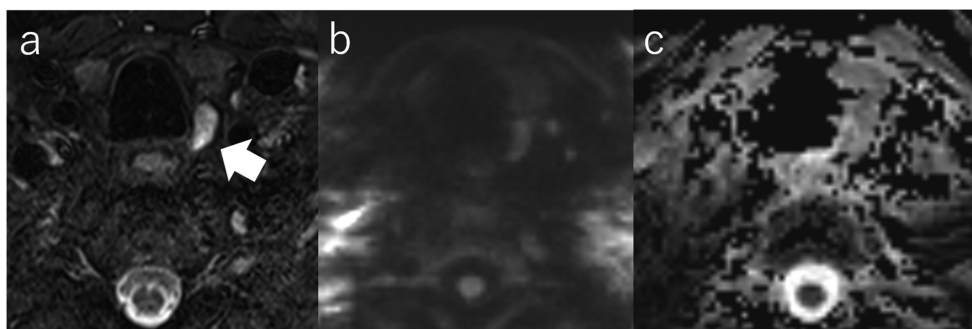


**Fig. 2** Representative RS-EPI images of a 72-year-old woman with primary hyperparathyroidism. **a:** STIR: A high-intensity mass on STIR was detected behind the left lobe of the thyroid gland. **b:** DWI with RS-EPI: A high-intensity lesion on DWI was detected in the corresponding location on STIR. The lesion was evaluated as showing almost no or faint distortion. **c:** ADC map: A high value was detected on the ADC map. The lesion was diagnosed as a PTA of the left-inferior gland. A 28 × 22 × 5 mm PTA was confirmed at surgery.

having a PTA of the right-inferior gland and presented high-intensity mass on STIR; however, there was considerable distortion on SS-EPI (Fig. 1). In contrast, in the case of a 72-year-old woman with a PTA at the left-inferior gland with DWI using RS-EPI, the lesion was identified with less distortion (Fig. 2). In the case of a 25-year-old woman, <sup>99m</sup>Tc-sestamibi scintigraphy could not be taken because she was in lactation (This case was excluded from the study because of the DWI acquisition using a different *b* value). MRI showed PTA in the left

paratracheal region of upper mediastinum, and iso-signal was detected on the ADC map (Fig 3). No complications such as recurrent nerve palsy were observed in all patients including these cases.

#### Discrimination of PTAs from the thyroid gland and cervical lymph nodes using ADCs

The PTAs exhibited relatively high signal intensity on DW-MRI with either SS-EPI or RS-EPI, with high ADC values. On SS-EPI, the average ADC values of the PTAs, thyroid glands, and

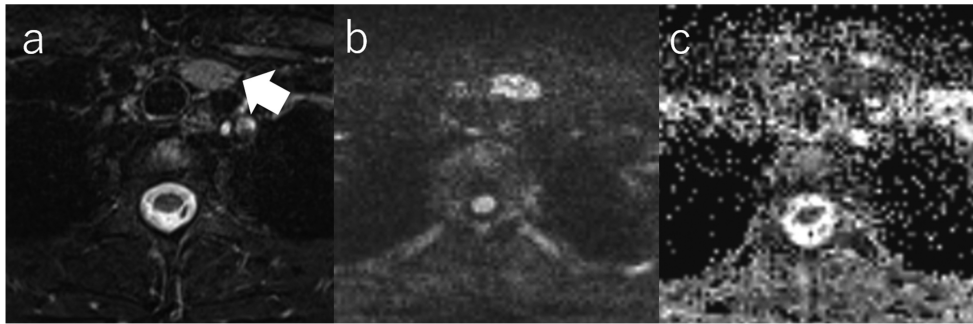


**Fig. 3** Representative RS-EPI images of a 25-year-old woman with primary hyperparathyroidism. **a:** STIR: An iso-intensity mass on STIR was detected in the left-paratracheal region of the upper mediastinum. **b:** DWI with RS-EPI: A high-intensity lesion on DWI was detected in the corresponding location on STIR. **c:** ADC map: An iso signal was detected on the ADC map. The lesion was diagnosed as a PTA of the left-inferior gland. Although the lesion was small ( $12 \times 6 \times 6$  mm), PTA was confirmed during surgery.

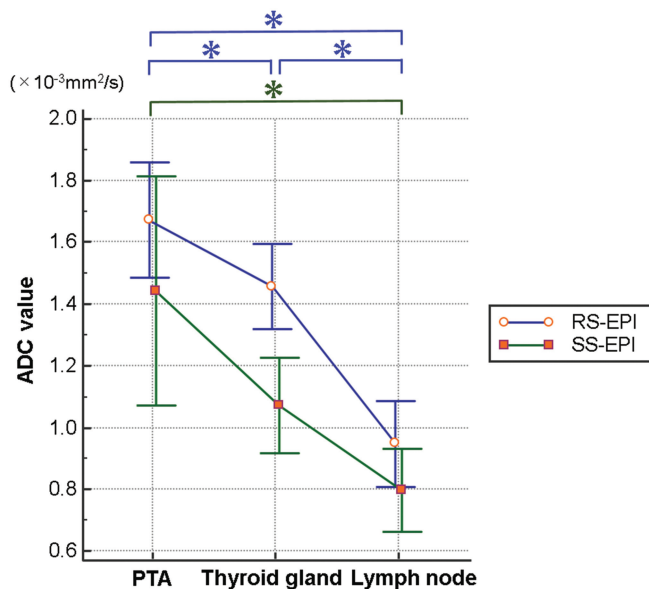


**Fig. 4** The ADC values of the parathyroid lesions, thyroid glands, and cervical lymph nodes. Green line: SS-EPI. Blue line: RS-EPI. \* $P < 0.05$ . RS-EPI, readout-segmented echoplanar imaging; SS-EPI, single-shot echo-planar imaging.

cervical lymph nodes were  $1.44$ ,  $1.07$ , and  $0.80 \times 10^{-3} \text{ mm}^2/\text{s}$ , respectively, and a significant difference between the PTAs and lymph nodes was observed. Moreover, the average ADC values of the PTAs, thyroid glands, and cervical lymph nodes were  $1.67$ ,  $1.46$ , and  $0.95 \times 10^{-3} \text{ mm}^2/\text{s}$  on RS-EPI, and the PTAs exhibited significantly higher ADC values compared to those of the thyroid glands and lymph nodes (Fig. 4).

## Discussion

We evaluated the clinical utility of DWI for the preoperative localization of PTAs. While the PTAs were faintly identified with intense distortion on 1.5T SS-EPI, they were fairly identified with moderate distortion on 3T RS-EPI. The

inter-rater reliability was substantial or perfect, and the validity of DW-MRI for the localization of PTAs was demonstrated. In addition, the PTAs could be discriminated from cervical lymph nodes and thyroid glands by measuring the ADC values, and thus, RS-EPI is expected to become the optimal diagnostic modality for the localization of PTAs.

With the introduction of 3T MRI, improved diagnostic performance for the detection of PTAs has been reported in relation to the higher spatial resolution and contrast-to-noise ratio.<sup>1</sup> PTAs are usually T2 hyperintense, and fat suppression is effective to achieve an accurate depiction.<sup>1</sup> However, fat suppression is not easy to use in the neck region, especially in the mediastinum, because of the magnetic field inhomogeneities due to the proximity of lungs and upper airways.<sup>19</sup> Thus, it remains challenging to obtain good images of PTAs with MRI, and there is currently no consensus on the optimal MRI protocol for the evaluation of PTAs.

The diagnostic value of 4D MRI and of the IDEAL sequence for the detection of PTAs has been reported.<sup>20,21</sup> Although the use of these imaging techniques improved the diagnostic sensitivity for the detection of PTAs, false-positive diagnoses are occasionally attributed to cervical lymph nodes or adjacent/ectopic thyroid tissues. To distinguish PTAs from lymph nodes and thyroid tissues, Yildiz et al. used conventional DWI provided by a 1.5T system, and they reported higher ADC values in parathyroid lesions compared to lymph nodes and thyroid tissues; however, the statistical significance of these differences was not reported.<sup>9</sup>

Although SS-EPI is a well-established conventional method for the acquisition of DWI data with short scan times, it suffers from susceptibility artifacts, leading to geometric distortion, signal dropout, and image blurring, which occur especially at higher field strengths such as 3T.<sup>10</sup> Alternatively, RS-EPI is a multi-shot sequence that reduces susceptibility artifact and blurring arising from T2\* decay, and thus, lower distortion can be achieved.<sup>22</sup> The clinical utility of RS-EPI has been well documented in some regions, including the head and neck.<sup>13</sup> In our present case series, the

acquisition parameters were quite different between RS-EPI and SS-EPI because they were independently set to optimize their image quality within clinically acceptable acquisition times (2–3 min). Since a sufficient SNR was not expected for SS-EPI, the number of excitations was increased to four. A sufficient SNR was expected for RS-EPI, so we increased the number of readout segments to five, to reduce the distortion. The results demonstrated that RS-EPI showed less distortion and better identification of PTA than the 1.5T SS-EPI, and the conclusions of the two independent readers showed good correlation. Because of its retrospective design and ethical issues (limited acquisition time), it was not possible to perform a direct comparison between SS-EPI and RS-EPI under the same magnetic field strength. However, given that the distortion level due to magnetic field inhomogeneities increases with field strength, RS-EPI is thought to be more beneficial in obtaining less distorted images at 3T compared to SS-EPI.

RS-EPI is thought to be a useful and reliable imaging technique for the evaluation of PTAs. However, we observed herein that, even with RS-EPI, some PTAs were poorly identified with intense distortion, which might mask the improvement in the lesion identification score. The distortion might come from (1) the relatively large FOV needed to obtain whole neck images, (2) susceptibility artifact that remained even with RS-EPI, and/or (3) motion artifact from respiration. In addition, it is not still easy to obtain good-quality DW images at the upper mediastinum due to the complex stricture facing the air, and the establishment of a feasible imaging protocol of the cervical region to the upper mediastinum using DW-MRI is expected.

In this study, we used ADC values for discriminating the PTAs and other cervical organs, and the PTAs were well distinguished from the thyroid glands and cervical lymph nodes. Cervical lymph nodes exhibit low ADC values,<sup>23</sup> and benign neck pathologies including adenomas are reported to show relative high ADC values,<sup>24,25</sup> which are consistent with our present observations. Higher ADC values were observed on RS-EPI compared with SS-EPI in our case series. Differences in ADC values between RS-EPI and SS-EPI are still controversial. Although higher ADC values on RS-EPI have been reported in the human mammary gland and in a phantom study,<sup>22,26</sup> Koyasu et al. reported no significant differences in the ADCs of salivary gland lesions.<sup>13</sup> In our present cases, the accurate evaluation of lesions due to less distortion on 3T RS-EPI may have contributed to the precise selection of the area, while more distorted lesions on 1.5T SS-EPI might have been contaminated by surrounding fat tissue and consequently resulted in a decreased ADC, which we observed particularly in the thyroid glands. Adding DWI using RS-EPI to common sequences such as STIR and T2WI enable more accurate localization diagnosis and reduce the surgical complications such as recurrent nerve palsy, and be beneficial for the preoperative evaluation for patients with PTAs who cannot undergo 99mTc-sestamibi

scintigraphy due to pregnancy or lactation because of the lack of radiation exposure.

This is the first study to investigate the clinical utility of RS-EPI in the preoperative localization of PTAs, to our knowledge. Although MRI does not substitute for MIBI scintigraphy or US at this moment, we believe that our results indicated added value and future potential of RS-EPI in localization of PTAs. One of the limitations of our study was its retrospective design. In addition, the acquisition protocols for SS-EPI and RS-EPI were independently set to maximize their own features (rather than a comparison of the two protocols), which resulted in different acquisition schemes. The sample size was small, and there would be a selection bias because selected patients with surgically confirmed pathologies were included. Further prospective studies with larger sample sizes are warranted to clarify the diagnostic utility, indications, and limitations of RS-EPI for the localization of PTAs.

## Conclusion

Our study demonstrated that 3T RS-EPI produces images with less DWI distortion than 1.5T SS-EPI, which may provide clinical advantages in the localization of PTA. And PTAs have higher diffusion properties compared with thyroid glands and cervical lymph nodes using RS-EPI. This feature enables us to the differentiation of PTAs from nearby structures on MRI.

## Acknowledgments

We sincerely thank Denis Le Bihan and Yuta Urushibata for their valuable advice on the manuscript.

## Funding

This study was funded in part by Grants-in-aid for Scientific Research from the Japan Society for the Promotion of Science.

## Conflicts of Interest

The authors declare that there are no conflicts of interest for this study.

## References

1. Argirò R, Diacinti D, Sacconi B, et al. Diagnostic accuracy of 3T magnetic resonance imaging in the preoperative localization of parathyroid adenomas: comparison with ultrasound and 99mTc-sestamibi scans. *Eur Radiol* 2018; 28:4900–4908.
2. Bartsch D, Nies C, Hasse C, Willuhn J, Rothmund M. Clinical and surgical aspects of double adenoma in patients with primary hyperparathyroidism. *Br J Surg* 1995; 82:926–929.
3. Smit PC, Borel Rinkes IH, van Dalen A, van Vroonhoven TJ. Direct, minimally invasive adenomectomy for primary

- hyperparathyroidism: An alternative to conventional neck exploration? *Ann Surg* 2000; 231:559–565.
4. Sackett WR, Barraclough B, Reeve TS, Delbridge LW. Worldwide trends in the surgical treatment of primary hyperparathyroidism in the era of minimally invasive parathyroidectomy. *Arch Surg* 2002; 137:1055–1059.
  5. Nael K, Hur J, Bauer A, et al. Dynamic 4D MRI for characterization of parathyroid adenomas: Multiparametric analysis. *AJNR Am J Neuroradiol* 2015; 36:2147–2152.
  6. Kunstman JW, Kirsch JD, Mahajan A, Udelsman R. Parathyroid localization and implications for clinical management. *J Clin Endocrinol Metab* 2013; 98:902–912.
  7. Ruf J, Lopez Hänninen E, Steinmüller T, et al. Preoperative localization of parathyroid glands: Use of MRI, scintigraphy, and image fusion. *Nucl Med (Stuttg)* 2004; 43:85–90.
  8. Wakamatsu H, Noguchi S, Yamashita H, et al. Parathyroid scintigraphy with  $^{99m}\text{Tc}$ -MIBI and  $^{123}\text{I}$  subtraction: A comparison with magnetic resonance imaging and ultrasonography. *Nucl Med Commun* 2003; 24:755–762.
  9. Yildiz S, Aralasmak A, Yetis H, et al. MRI findings and utility of DWI in the evaluation of solid parathyroid lesions. *Radiol Med (Torino)* 2019; 124:360–367.
  10. Walter SS, Liu W, Stemmer A, et al. Combination of integrated dynamic shimming and readout-segmented echo planar imaging for diffusion weighted MRI of the head and neck region at 3 Tesla. *Magn Reson Imaging* 2017; 42:32–36.
  11. Porter DA, Heidemann RM. High resolution diffusion-weighted imaging using readout-segmented echo-planar imaging, parallel imaging and a two-dimensional navigator-based reacquisition. *Magn Reson Med* 2009; 62:468–475.
  12. Porter DA, Calamante F, Gadian DG, Connelly A. The effect of residual Nyquist ghost in quantitative echo-planar diffusion imaging. *Magn Reson Med* 1999; 42:385–392.
  13. Koyasu S, Iima M, Umeoka S, et al. The clinical utility of reduced-distortion readout-segmented echo-planar imaging in the head and neck region: initial experience. *Eur Radiol* 2014; 24:3088–3096.
  14. Klingebiel M, Ullrich T, Quentin M, et al. Advanced diffusion weighted imaging of the prostate: Comparison of readout-segmented multi-shot, parallel-transmit and single-shot echo-planar imaging. *Eur J Radiol* 2020; 130:109161.
  15. Kishimoto AO, Kataoka M, Iima M, et al. Evaluation of malignant breast lesions using high-resolution readout-segmented diffusion-weighted echo-planar imaging: Comparison with pathology. *Magn Reson Med Sci* 2021; 20:204–215.
  16. Landis JR, Koch GG. An Application of hierarchical kappa-type statistics in the assessment of majority agreement among multiple observers. *Biometrics* 1977; 33:363–374.
  17. McHugh ML. Interrater reliability: The kappa statistic. *Biochem Med (Zagreb)* 2012; 22:276–282.
  18. Kanda Y. Investigation of the freely available easy-to-use software “EZR” for medical statistics. *Bone Marrow Transplant* 2013; 48:452–458.
  19. Grayev AM, Gentry LR, Hartman MJ, Chen H, Perlman SB, Reeder SB. Presurgical localization of parathyroid adenomas with magnetic resonance imaging at 3.0 T: An adjunct method to supplement traditional imaging. *Ann Surg Oncol* 2012; 19:981–989.
  20. Memeh KO, Palacios JE, Khan R, Guerrero MA. Preoperative localization of parathyroid adenoma: Performance of 4d mri parathyroid protocol. *Endocr Pract* 2019; 25:361–365.
  21. Ozturk M, Polat AV, Celenk C, Elmali M, Kir S, Polat C. The diagnostic value of 4D MRI at 3T for the localization of parathyroid adenomas. *Eur J Radiol* 2019; 112:207–213.
  22. Kanao S, Kataoka M, Iima M, et al. High-resolution diffusion-weighted MRI of the breast using readout-segmented EPI and single-shot EPI. *Imaging Med* 2017; 9:185–190.
  23. Moreau B, Iannessi A, Hoog C, Beaumont H. How reliable are ADC measurements? A phantom and clinical study of cervical lymph nodes. *Eur Radiol* 2018; 28:3362–3371.
  24. Kanmaz L, Karavas E. The role of diffusion-weighted magnetic resonance imaging in the differentiation of head and neck masses. *J Clin Med* 2018; 7:130.
  25. Srinivasan A, Dvorak R, Perni K, Rohrer S, Mukherji SK. Differentiation of benign and malignant pathology in the head and neck using 3T apparent diffusion coefficient values: Early experience. *AJNR Am J Neuroradiol* 2008; 29:40–44.
  26. Ihalainen T, Kuusela L, Soikkeli M, Lantto E, Ovissi A, Sipilä O. A body-sized phantom for evaluation of diffusion-weighted MRI data using conventional, readout-segmented, and zoomed echo-planar sequences. *Acta Radiol* 2016; 57:947–954.